NASA Technical Memorandum 86760

NASA TM 86760

NASA-TM-86760 19850024864

A Review of Shock Waves Around Aeroassisted Orbital Transfer Vehicles

Chul Park

June 1985

National Aeronautics and Space Administration

NASA Technical Memorandum 86760

A Review of Shock Waves Around Aeroassisted Orbital Transfer Vehicles

Chul Park, Ames Research Center, Moffett Field, California

June 1985

National Aeronautics and
Space Administration

Ames Research Center
Moffett Field California 94035

A REVIEW OF SHOCK WAVES AROUND AEROASSISTED ORBITAL TRANSFER VEHICLES

Chul Park

Ames Research Center

SUMMARY

Aeroassisted orbital transfer vehicles (AOTVs) are a proposed type of reusable spacecraft that would be used to transport cargoes from one Earth-bound orbit to another. Such vehicles could be based on the proposed Space Station and used to transport commercial satellites from the Space Station to geostationary orbits or to polar orbits and return. During a mission, AOTVs would fly through Earth's atmosphere, thus generating aerodynamic forces that could be used for decelerating the vehicles or changing their direction. This review of published AOTV research findings was concerned with the shock-wave-induced, high-temperature airflows that would be produced around these vehicles during atmospheric flight. In the survey, special emphasis was placed on the problems of (1) the chemical physics of multitemperature, ionizing, nonequilibrium air flows, and (2) the dynamics of the flows in the base region of a blunt body with complex afterbody geometry.

SYMBOLS

AOTV aeroassisted orbital transfer vehicle

C_d drag coefficient

C_p specific heat at constant pressure

C_v specific heat at constant volume

c.g. center of gravity

g gravitational acceleration of the Earth = 9.80 m/sec^2

GEO geosynchronous Earth orbit

HEO high Earth orbit

I_p peak radiation intensity behind shock

LEO low Earth orbit

L/D lift-to-drag ratio

M	mass of vehicle
M_a	mass of air displaced by a vehicle
M_f	final mass of a vehicle at end of a rocket engine burn
M_i	initial mass of a vehicle at the beginning of rocket engine burn
OTV	orbital transfer vehicle (without aeroassist)
p_s	stagnation pressure
p_∞	free-stream pressure
q_c	convective heat-transfer rate, kW/m^2
q_r	radiative heat-transfer rate, kW/m^2
R	nose radius, m
RCS	reaction control system
T	heavy-particle translational temperature
T_e	electron translational temperature
T_r	heavy-particle rotational temperature
T_v	vibrational temperature
t	time, sec
V	flight velocity, m/sec
V_f	vehicle velocity at end of rocket engine burn or of aerobrake
V_i	vehicle velocity at beginning of rocket engine burn or of aerobrake
V_j	exhaust velocity of rocket engine, m/sec
x	distance from shock
x_e	distance for chemical equilibrium behind shock, where radiation intensity is 1.1 times the plateau value
x_p	distance for peak radiation intensity behind shock
γ	C_p/C_v

ΔV $V_f - V_i$

λ mean free path

μ viscosity

ρ free-stream density, kg/m^3

INTRODUCTION

Starting about 1970, near-Earth space became a realm not only for scientific exploration but also for commercial enterprises. The most notable commercial use of space is in telecommunications. For the nations fortunate enough to be located in relatively low latitudes, the geosynchronous satellites, located 42,210 km away from Earth's center, provide a relatively inexpensive means of transferring information from one ground position to another over a large distance. For the nations that are located near the North or the South Poles, high satellite orbits that can serve similar purposes have been found and are being used. These high-Earth-orbit (HEO) satellites are used not only for telecommunications, but also, for example, in making weather and crop forecasts; detecting crop-destroying insects and diseases; finding new Earth resources, such as natural gas or oil; detecting shipwrecks and forest fires; and space manufacturing. In addition to these HEO satellites, there are some scientific satellites that are in low-Earth-orbits (LEO), either over or near the Poles. Delivering satellites from the ground to these various orbits became a profitable commercial activity, and, in some instances, it has been shown that retrieving defunct satellites could also be done profitably.

Various nations have developed different rocket vehicles for the purpose of carrying such satellite cargoes. Most of these vehicles are still in development, and so it is difficult to assess and compare their performance on a common basis. In addition, because they are in the process of development, a great deal of pertinent information about them is still proprietary. This makes the task of reviewing the subject matter rather difficult. Under this constraint, therefore, the present author chooses two basic guidelines: (1) any information available to the general public without restriction will be freely referred to, and (2) the author will freely upgrade available performance data if, in his opinion, such upgrading can be considered a reasonable certainty.

Figure 1 shows two such typical carrier vehicles: the U.S. Space Shuttle and Ariane of European Space Agency (ref. 1). The Ariane Vehicle is shown here with four solid-fuel boosters, even though such a combination has not yet been flown. In the opinion of the author, adding four boosters in this way seems to be a reasonably easy thing to do. As shown in the figure, the Space Shuttle and Ariane are expected to deliver, respectively, with the anticipated upgrading, about 30,000-kg and 4,500-kg payloads to LEOs.

To transfer such payloads to an HEO, such as a geostationary Earth orbit (GEO), additional propulsion is necessary. In figure 1, the upper stage vehicle for Ariane is visible as the top part of the assembly. For the Space Shuttle, the additional stage is stowed inside the cargo bay of the Orbiter and does not appear in the figure. The payload that can be delivered to an HEO will be determined principally by the specific impulse of the rocket engine of the upper stage vehicle. The specific impulses of the systems vary greatly depending on the fuel used. The liquid fueld that do not require cryogenic cooling (which are known commonly as storable fuels), deliver specific impulses of about 250 sec; liquid hydrogen, which requires cryogenic cooling, can deliver a specific impulse of the order of 450 sec (ref. 2). At this time, one cannot judge the relative merits of these fuels. For purposes of this review, therefore, a specific impulse of 350 sec (the average between the high and the low) will be assumed. The corresponding exhaust velocity V_j, which is by definition a product of g (Earth's gravitational acceleration) and specific impulse, becomes

$$V_j = 3{,}430 \text{ m/sec} \tag{1}$$

The final payload will depend partly also on where the vehicle is launched. For example, the least fuel is required for launches from the Equator. In the interest of simplicity, therefore, equatorial launches will be assumed in this analysis.

To transfer from a LEO to a GEO, one must follow an elliptic orbit with perigee and apogee coinciding with the LEO and GEO, as shown in figure 2. The average circular velocity around the center of Earth is well known: at an altitude of 150 km (LEO), it is 7,768.5 m/sec; at an altitude of 42,210 km (GEO), it is 3,069.8 m/sec. For the elliptic orbit with perigee at 150 km (LEO) and apogee at 42,210 km (GEO), the perigee velocity at an altitude of 150 km (LEO) is 10,342.4 m/sec; and the apogee velocity at an altitude of 42,210 km (GEO) is 1,580.7 m/sec. In order to transfer from the circular orbit at LEO to the elliptic transfer orbit, therefore, a velocity increment ΔV ($=V_f - V_1$) of 2,573.9 m/sec is necessary. After reaching the GEO, there must be another velocity increment ΔV of 1,489.0 m/sec in order to stay in the circular orbit.

The well-known rocket equation relates the velocity increment ΔV to the required mass of fuel by

$$M_1/M_f = \exp(\Delta V/V_j) \tag{2}$$

where M_1 is the initial mass, which includes the mass of the expended fuel, and M_f is the final mass. For the case under consideration, the mass ratios become

$$\text{For perigee burn : } M_i/M_f = 2.118 \tag{3}$$

$$\text{For apogee burn : } M_i/M_f = 1.544 \tag{4}$$

$$\text{The mass ratio product} = 2.118 \times 1.544 = 3.270 \tag{5}$$

At present, the upper stage vehicles used for this purpose are expendable, that is, they are discarded after one use (see fig. 2(a)). This expendable upper stage is becoming expensive for the following reasons: (1) the cost of manufacturing and testing, and (2) relatively high insurance premiums because of low reliability. By making the upper stage vehicle reusable, one could eliminate both these problems and achieve a considerable commercial advantage. Such a conceptual vehicle, operating solely on rocket engines for producing ΔV's, as depicted in figure 2(b), is referred to as orbital transfer vehicle (OTV) (ref. 3).

The OTVs suffer from one serious handicap, however. After delivering the payload to the GEO, the OTV must now expend the mass ratio of 3.270, the same mass ratio as for the ascent, in order to descend to the LEO. Since there is a fixed mass for the engines, fuel tanks, and control and command components, this mass ratio requirement of 3.270 greatly reduces the true payload capacity of the OTV.

The idea of aeroassisted orbital transfer vehicle (AOTV) was initiated originally to alleviate this difficulty (refs. 4,5). An AOTV would be equipped with an aerodynamic surface that would produce drag (and some lift, if possible) and withstand whatever heat it would be exposed to. On return from the GEO, the AOTV would dive into Earth's atmosphere and skip out of it as shown schematically in figure 2(c). In doing so, the vehicle would be decelerated by drag, an operation referred to as aerobraking. A small course adjustment would be necessary after the vehicle skipped out of the atmosphere, but it could be accomplished by using only a very small amount of fuel. By this operation, the mass ratio required for the return trip is reduced from 3.27 to about 1.55, an advantage of a factor greater than 2. Though this type of AOTV theoretically requires no lift, a small amount of lift is needed in reality because of the need to correct for the unforeseen deviation of the flight course from the planned course. We can call this class of AOTV low-lift AOTVs or aerobraking AOTVs.

The advantages of the AOTV can be determined fairly easily (by using eqs. (1)-(5)) if one knows, for example, the weight of the hardware (rocket engine, fuel tanks, and the command and control components) and the starting mass at the LEO. Before making such calculations, however, one must first recognize that an OTV and AOTV have three different applications: (1) delivery of payloads from LEO to GEO, (2) retrieval of payloads from GEO to LEO, and (3) excursions to GEO in which no transfer of payload takes place. A retrieval may be required if it is necessary to bring a malfunctioning satellite back to the Space Station or to Earth for repair. An excursion mission may suffice if the required repair is simple enough that it could be accomplished in orbit. By adding and multiplying the numbers given in equations (1) to (5), one obtains the payload capacities for these three functions, as shown in table 1. The values in table 1 are based on the following assumptions: that the LEO is on an equatorial plane, that the rocket engine has V_j given by equation (1), and that the small amount of fuel necessary for minor course adjustments is neglected. As shown in the table, an AOTV can improve the payload capacity considerably over that of an OTV, although the maximum deliverable payload by an AOTV is still less than that of an expendable rocket under the given assumptions. An expendable rocket cannot perform the second and the third functions

at all, however. Besides, an AOTV can deliver payloads greater than that of an expendable vehicle simply by carrying extra fuel in an expendable fuel tank. For an AOTV, the LEO takeoff mass of 30,000 kg can be exceeded with no adverse effect; by attaching any number of expendable fuel tanks, the takeoff mass can be increased without a limit. One interesting point to note in table 1 is that the maximum mass of the AOTV at the time of atmospheric entry is of the order of 10,000 kg. Detailed calculations of this type have been carried out by various authors in recent years and are available in the open literature (refs. 6-12).

Another reason for proposing an AOTV is for changing orbital inclination angle with respect to the equator (refs. 4,5). To illustrate this point, let us imagine a satellite in an equatorial orbit at the altitude of 150 km with a circular velocity of 7,768 m/sec. For some reason, it is desired to change to a polar orbit. The required ΔV is $1.4142 \times 7{,}768 = 10{,}986$ m/sec, as indicated in figure 3. If this ΔV is achieved entirely by burning rocket fuel, the required mass ratio is 22.60. If the vehicle is to return from the polar orbit back to the equatorial orbit, the required mass ratio is $22.60 \times 22.60 = 605.4$. Such a large mass ratio requirement could be reduced if the vehicle could utilize aerodynamic lift. Assuming that the vehicle had an aerodynamic lifting surface, it could dive into the atmosphere with an expenditure of a small amount of fuel. The vehicle would fly in a highly banked attitude so as to produce a large sidewise force. This sidewise force could make the necessary direction change efficiently. This operation is referred to as aeromaneuvering (ref. 4). The vehicle would slow down during this aeromaneuvering flight because of its drag. This velocity decrement must be compensated for by a propulsive means, that is, by operating a rocket or an air-breathing engine. Therefore, the amount of fuel necessary to make a given angle turn would be inversely proportional to the lift-to-drag ratio L/D of this vehicle. As was true for the aerobraking AOTV, this maneuvering vehicle must skip out of the atmosphere and attain and desired altitude expending a small amount of fuel also. For this type of vehicle, a large L/D is preferred, and it can be designated a high-lift AOTV, or an aeromaneuvering AOTV.

Unlike the aerobraking AOTV, the benefits of an aeromaneuvering AOTV are not easy to predict for missions involving large orbital-plane-angle changes because there are too many arbitrary parameters that affect the payload calculation: little such information appears in the open literature (refs. 4,8,9). Hence, no attempt will be made here to assess the benefits of the high-lift AOTV for this kind of application. However, a high-lift AOTV can be designed to perform all the functions of a low-lift AOTV, in addition to its special capability (ref. 13). Consequently, much of the following discussion is also pertinent to the high-lift AOTV.

FLIGHT REGIMES

Since there is no reason for the AOTVs to land on the ground, the most economic way of operating them would be to base them in space--on the proposed Space Station (ref. 14) or on some similar space structure. This means that the Space Shuttle

need transport the AOTV from Earth to space only once. Thereafter, the Space Shuttle would only carry the ultimate payload cargo (satellite) and the fuel needed by the AOTV. The AOTV fuel could usually be transported without difficulty, because on most of its missions, the cargo-capability of the Shuttle is not filled. When the Space Shuttle reached the Space Station, it could transfer the AOTV fuel into a large fuel-storage facility. In this way, the load-factor for the Space Shuttle could be maintained at close to 100%. When an AOTV took off from the Space Station, it would start from zero-g. Hence, its rocket engine could be arbitrarily small in comparison with the weight of the assembled AOTV. (When a rocket takes off from the ground, it must at least overcome Earth's gravity.) The optimum size and thrust of the rocket engine can be determined from other constraints, free from the requirement that it be greater than the takeoff weight.

Such a space-based, reusable AOTV demands, however, that most parts of the vehicle be reusable, with only minimum maintenance. One of the most critical components of the AOTV that must meet this requirement is the aerodynamic surface (the aerobrake for the low-lift AOTV or the lifting surface for the high-lift AOTV). The aerodynamic surface will be subject to heat transfer from the hot shock layer flow around it. To be maintenance-free, such a surface must not only withstand the heat but be chemically unaffected by atomic oxygen that exists in the shock layer flow. Presently, such materials are used on the Space Shuttle Orbiter (refs. 15,16). These materials can withstand heat-transfer rates of the order of 200 kW/m^2. For this review, therefore, it will be assumed that the tolerable heat-transfer rate is 200 kW/m^2.

In order to roughly define the regime of flight of the AOTVs, we will assume the AOTV to be a sphere, which has no lift, and the drag coefficient, calculated from the Newtonian theory, to be $C_d = 1$. Equations of motion of such a body are well known (ref. 17). We will assume that the AOTV is returning from the GEO, and that its mass is 10,000 kg, a typical maximum value seen in table 1. After the vehicle skips out of the atmosphere, we will assume that its new apogee will be 200 km above the ground. As a trial value, we will assume the radius of the sphere to be 10 m. The convective heat-transfer rate to the stagnation point of a sphere can be approximated by

$$q_c = 5.14 \times 10^{-8} (\rho/R)^{1/2} V^{3.15} \ kW/m^2 \qquad (6)$$

where ρ is free-stream density in kilograms per cubic meter, R is nose radius in meters, and V is flight velocity in meters per second (ref. 18). Figure 4 shows the results of the calculation. As seen here, this vehicle approximately satisfies the maximum allowed heat-transfer limit of 200 kW/m^2. Its perigee is approximately 80 km.

One wonders how the nose radius R affects the convective heat-transfer rates. According to equation (6), the heat-transfer rates are inversely proportional to the square root of the nose radius. However, this is not really true here. For an AOTV, there exists an implicit relationship between the flight density ρ and the nose radius R imposed by the fact that the velocity decrement

through the aerobraking flight be the desired value. To illustrate this relationship, one begins with the equation of motion along the flightpath in the form

$$M \frac{dV}{dt} = -(1/2)C_d \rho V^2 \pi R^2 \tag{7}$$

Integration of equation (7) leads to

$$V_f/V_i = \exp(-0.5M_a/M) \tag{8}$$

where V_i and V_f are the velocities of the AOTV at the time of entry into and exit from Earth's atmosphere, and M_a is the mass of air displaced by the AOTV:

$$M_a = \int \pi R^2 \rho V \, dt$$

Since the ratio V_f/V_i is fixed at approximately 0.75, equation (8) leads further to

$$M_a = 0.572 \times M \tag{9}$$

That is, an AOTV must displace an air mass that is about 57% of its own mass. In order to accomplish this, the density regime an AOTV chooses to fly must be inversely proportional to the square of its radius R, that is,

$$\rho = \text{const}/R^2 \tag{10}$$

By introducing equation (10) into equation (6), one obtains the scaling relationship

$$q_c = \text{const} \times V^{3.15} R^{-1.5} \tag{11}$$

Equation (11) shows that the convective heat-transfer rate is relatively sensitive to the choice of nose radius: one cannot vary the nose radius too far from the value of 10 m we determined earlier.

Conversely, because of equation (10), the flight density is also sensitively affected by the nose radius: one cannot vary the perigee height too far from the value of 80 km we determined earlier. The flight regimes are, therefore, fairly narrowly defined. These are shown in table 2 at the perigee for an aerobraking AOTV with zero lift.

More detailed analyses of the trajectories and the associated flight regime parameters have been performed analytically (ref. 19). Such calculations include the effects of variations in nose radius, allowable heat-transfer rate value, and lift-to-drag ratio L/D. The results of these analyses, as well as the numberical calculations referred to earlier (refs. 6-12), indicate that these additional

parameters affect the flight regime parameters relatively weakly. Hence, for the purpose of this review, the parameters given in table 2 will be used throughout for the aerobraked AOTVs.

CHEMICAL KINETICS AND RADIATIVE HEAT-TRANSFER RATES

The shock standoff distance for a sphere is a function of the density ratio across the normal shock wave, or, equivalently, a function of the effective specific heat ratio $\gamma = C_p/C_v$ (see, e.g., ref. 20). The relationships among the three parameters are well known for an inviscid flow. Since the characteristic Reynolds number for an aerobraked AOTV is relatively large (1.5×10^5 in the typical conditions shown previously), the inviscid assumption may be applicable in estimating the shock standoff distance. However, the density ratio is a strong function of the chemical state behind the shock wave, which is yet to be determined. If the chemistry is frozen behind the shock wave, the density ratio is 6, and the shock standoff distance for a sphere of 10 m radius would be about 1.2 m. If the flow behind the shock is in equilibrium, it would be about 0.4 m. In the low-density regime of interest, however, the chemical state is most likely in the process of chemical relaxation, that is, vibrational excitation, dissociation, and ionization. For this reason, neither of these standoff distance values would be valid for the AOTV.

There is one well-known standardized computer program that computes chemical reactions for a one-dimensional inviscid flow (ref. 21), and one might think that the chemical state behind the shock could be estimated by operating such a computer program. Unfortunately, such existing programs assume that all internal modes of energy (rotation, vibration, electronic excitation, and electron translational) are in equilibrium with the translational mode of the heavy particles, that is, with the gas temperature. This one-temperature assumption was believed to be valid for most past applications. It is well known that rotational temperature equilibrates with translational temperature very quickly (ref. 22). Vibrational excitation is somewhat slower, but in the environments encountered in past space missions, it was usually faster than the rates of dissociation (ref. 23). Both the vibrational relaxation rates and dissociation rates are proportional to density, but dissociation rates are more strongly dependent on translational temperature than the vibrational relaxation rate. At temperatures below about 10,000 K, typically, vibrational excitation is finished before any significant dissociation can occur (ref. 23). For the AOTV, however, the translational temperature behind the shock is over 40,000 K. Hence, vibrational relaxation and dissociation are likely to proceed simultaneously.

It is known also that electron kinetic temperature interacts strongly with the vibrational modes of a molecule (ref. 24). If there is any ionization or dissociation by impacts of electrons, the energy content in electron gas is reduced by the corresponding amount. The equilibration between the electron translational temperature and heavy-particle translational temperature is slow because of the large mass

disparity between them (refs. 25,26). This causes the electron translational temperature to deviate from the heavy-particle translational temperature.

Recent studies show that the low electronic states of atoms and molecules are easily excited to their Boltzmann values on impact by electrons (ref. 25). As a result, for the purpose of approximately determining the total energy contents in the electronic excitation mode, one may assume the electronic excitation temperature to be the same as the electron translational temperature.

For these reasons, the chemical reactions in the shock layer over an aerobraked AOTV requires, in general, the recognition of three different temperatures: heavy-particle translational and rotational, vibrational, and electronic excitation and electron translational (ref. 26). If the flow conditions were such that the interaction between the electron translational energy and vibrational excitation is allowed to proceed frequently, then one could further assume that the vibrational temperature and the electron-electronic temperature are the same, leading to a two-temperature situation (refs. 27-29).

To compute the reacting flows under this two- or three-temperature environment, reaction rate coefficients must be expressed in terms of these different temperatures. At present, very little is known of this multitemperature description of rate coefficients, although work is in progress in an effort to understand the phenomena (ref. 30).

This problem can be approached from a purely experimental viewpoint. Unfortunately, however, even the experimental data are contradicting and confusing. Beginning in the late 1950s and continuing until about 1970, shock tubes were operated to observe the flow behavior behind strong shock waves (refs. 31,32). Shock velocities in excess of 10 km/sec have been generated in such facilities. The free-stream densities in such tests were, however, typically 5 to 10 times higher than those given in table 2. In such tests, the intensity of radiation was measured with an instrument located outside the shock tube, looking through a window, as a function of the distance from the shock wave. The wavelengths of the observed radiation were varied over a wide range. In all such tests, it was found that the radiation intensity was zero at the shock wave, rose to a peak, and decayed and approached a plateau (see fig. 5(a)). The distance (or, equivalently, the time) to the peak x_p, the distance to the equilibration point x_e (defined as the point where radiation emission intensity becomes 1.1 times the plateau value), and the peak intensity value I_p have been measured over a wide range of conditions.

The peak intensity I_p was seen to be between about 2 and 15 times stronger than the plateau values, depending on the wavelength (ref. 31). This phenomenon became known as nonequilibrium overshoot, or nonequilibrium enhancement, of radiation. The quantities x_p, x_e, and I_p were found to approximately obey the so-called binary scaling law (refs. 31,32). That is, x_p and x_e were inversely proportional to the gas density, and I_p was proportional to density. As a result, when x_p and x_e were multiplied by the free-stream density and then plotted, all data fell within two narrow bands. The area under the intensity curve in figure 5(a), from $x = 0$ to $x = x_e$ became approximately independent of free-stream

density. This integrated intensity was referred to as nonequilibrium radiation intensity (ref. 31). Figure 5(b) shows schematically how the various temperatures might be varying to produce the observed radiative behavior.

The shaded areas in figure 6 show the experimentally determined x_p and x_e values (ref. 31). Until recently, there has not been any serious effort to quantitatively explain the observed data. Most recently, an effort was made to understand the observed phenomena, using the best available computing techniques. To do so, however, the form of dependence of various reaction rates on vibrational and electron-electronic temperatures had to be assumed (ref. 28). The results of such calculations are given in reference 28, and are reproduced in figure 6. The symbols in the figure show the results of the calculations obtained using various different chemical kinetic assumptions. Readers are referred to reference 28 for the meaning of the assumptions represented by each symbol. It is apparent from the figure that we are not yet able to quantitatively explain the observed nonequilibrium radiation enhancement phenomenon.

In figure 7, which is also reproduced from reference 28, the measured and calculated integrated intensity are compared in a similar manner. The calculated values are somewhat closer to the measured values in this plot than in figure 6, but are still not satisfactory. One notices also that the measured integrated intensities show scatter by a factor of nearly 4 at the most crucial velocity of 9 to 10 km/sec. (Although the perigee velocity is approximately 9 km/sec, the maximum radiation occurs slightly before perigee is reached, at which time the flight velocity is about 10 km/sec.) This extent of uncertainty is perhaps too large to be tolerated for the purpose of designing an AOTV.

In addition to the shock-tube experiments, flight experiments were conducted in the early years to investigate the chemical kinetic behavior in the shock layer over a reentry vehicle. Those flight-test projects are named Fire (refs. 33,34), Apollo (ref. 35), PAET (Planetary Atmospheric Experiment Test) (ref. 36), and RAM (Radio Attenuation Measurement)-C (refs. 37-41). The Fire vehicle was an approximately 1/4-scale model of the Apollo entry module. In both the Fire and Apollo experiments, the total radiation power incident on the stagnation region was measured, using several different instruments. In the PAET experiment, a multiple of narrowband monochromators were installed to measure the radiation incident on the stagnation region. In RAM-C test, microwave experiments (attenuation, reflection, and phase shift) were conducted to determine the behavior of electrons in the shock layer.

However, the results of these flight tests did not lead to any definite explanation or conclusion. In the case of Fire and Apollo, the radiative heat-transfer rates measured near an altitude of 80 km were much lower than those deduced from the shock-tube experiments. This observed phenomenon prompted a hypothesis known as "collision-limiting" (refs. 33-35). Radiation is a result of decaying of highly excited atoms and molecules into lower excited states. The excitation occurs as a result of collisions with particles (atoms, molecules, and electrons). The rates of such exciting collisions are proportional to gas density, and the rates of radiative decay are independent of gas density. By equating the rates of collisional

excitation and radiative decay rates, one finds that the radiation intensity decreases rapidly when the gas density is less than a certain critical value: there are not enough collisions to maintain the population of the highly excited states under this circumstance. That is, radiation intensity becomes "collision-limited." The nonequilibrium radiation data taken in shock tubes were obtained at densities higher than that at 80 km. If the collision-limiting phenomenon occurred at the altitude of 80 km, then the phenomenon could explain why the flight data were lower than those obtained in the shock tube. This explanation was accepted in the days of Apollo and was used in the design of Apollo missions.

In retrospect, however, this "collision-limiting" theory is flawed. In the Apollo days, one thought that the excitation of atoms and molecules occurred mostly through collisions of atoms and molecules. In recent years, it became known that electrons are many orders of magnitude more efficient in electronically and vibrationally exciting atoms and molecules (ref. 25). Using the available data on electron-impact excitation rates, one finds that the collision-limiting phenomenon occurs at altitudes of about 100 km (see ref. 25), instead of 80 km.

An alternative explanation of the observed low radiation intensity in Fire and Apollo is the effect of boundary-layer growth, which is known as the "truncation" hypothesis (ref. 31). According to this hypothesis, the profile of electron temperature may develop a thick, cool boundary layer near the wall owing to the high thermal conductivity of the electron gas. The electron temperature boundary layer may have grown so thick that it may extend almost to the shock wave, thereby preventing the occurrence of nonequilibrium overshoot in electron and vibrational temperatures. That is, the rise in radiation intensity is "truncated" by the cool, electron boundary layer. To prove the hypothesis, however, one must carry out a detailed fluid-mechanical calculation accounting for the multiple-temperature chemical kinetics, which is presently beyond our capability.

The PAET experiment (ref. 36) confirmed that the observed radiation at a selected wavelength (390 nm) was higher than the equilibrium value. Unfortunately, however, the experiment did not measure the global (integrated over the entire wavelength range) radiation. Also, the flight speed was considerably lower than that of AOTV. Analysis is in progress to explain quantitatively the values obtained in the PAET test, and has met with partial success. For a thorough verification, however, one must await generation of all the multitemperature rate coefficients mentioned earlier.

The results of the RAM-C test have been analyzed by several investigators (refs. 37-41). Each investigator was able to explain a portion of the data produced. However, there is no unifying analysis that explains all aspects of the data.

These uncertainties about chemical kinetics have a serious implication for the design of an aerobraked AOTV. If the shock-tube data shown in figure 7 are correct, the radiative heat-transfer rate q_r could be

$$40 \leq q_r \leq 400 \text{ kW/m}^2 \tag{12}$$

This additional heat-transfer rate imposes a serious burden on the heat shield. If the collision-limiting theory is correct, this large radiative heat-transfer rate will not occur; if the truncation theory is correct, however, this heat-transfer rate may have to be added to the convective rates of 200 kW/m^2 (see table 2) in the design of the heat shield. This is because, since the AOTV is larger than Apollo, the truncation phenomenon is less likely to occur for the AOTV than for Apollo.

To remove this uncertainty, three efforts must be undertaken simultaneously: (1) there must be a fluid-mechanical computer program that calculates flow field around a given multidimensional body, accounting for the effects of multitemperature chemical kinetics; (2) chemical and physical parameters needed in the above calculations must be generated; and (3) after computing the flow properties using the two items above, one must be able to compute radiative characteristics for the multitemperature nonequilibrium gas.

Of these three, task (3) is relatively the easiest. A computer program named HF730 was written in 1969 that allows differences among translational, rotational, vibrational, and electron temperatures (ref. 42). However, this program assumed a Boltzmann distribution of internal states at these given temperatures. In the nonequilibrium flow under consideration, the internal state populations are governed not by the Boltzmann relation but by one known as the "quasi-steady-state" relationship, which states that the sum of all electronic transitions into a state is approximately equal to the sum of all transitions going out of the state (ref. 25). A new computer program named NEQAIR (ref. 25) has been written by incorporating this principle into the HF730 program. The NEQAIR program requires a large set of excitation rate-coefficient values, only some of which are presently available; however, work is in progress in all these areas.

STABILITY, GUIDANCE, AND CONTROL

In the foregoing discussions, the aerobraking AOTV was assumed to be spherical and hence to have no lift. In practice, a small amount of lift is necessary for maneuvering. The velocity and flight angle at the time of atmospheric entry can be different from the planned values because of errors in the operation of the main rocket engines, both in thrust and in direction. In order to correct for any such errors, the vehicle must be maneuvered while in the atmosphere.

Also, it became known in recent years that the density of the atmosphere in the altitudes of interest can vary over a wide range, that is, nearly by a factor of 2 (refs. 17,43). The vehicle must be able to vary its flight altitude so that it satisfies equation (9). For these reasons, an aerobraking AOTV must maneuver to attain the required altitude. Lift capability would also be helpful in making small changes in orbital-plane inclination angle. For the Space Shuttle-Space Station system, the most likely LEO would be inclined 28.5° from Earth's equatorial plane (because the launch pad in Florida is in this inclined plane). By banking into the

appropriate side during the atmospheric flight, the vehicle could approach the target LEO orbit partially aerodynamically.

In space, a spacecraft's control of its attitude is accomplished by firing small rocket engines known as reaction control system (RCS) engines. An AOTV could use the RCS engines also for controlling its attitudes during atmospheric flight. To do so, however, it would be desirable to have a neutral stability in the mode to be controlled by an RCS engine. Otherwise, there will be an aerodynamic coupling between different modes (such as yaw-to-roll coupling).

To provide a neutral aerodynamic stability for an AOTV is not so easy, because the center of gravity (c.g.) will vary widely depending on the mission and on the amount of fuel remaining in the tanks. Since it is most likely that the vehicle will have a left-right symmetry, the c.g. variation will affect the pitching stability parameter most severely. These considerations lead to the conclusion that the primary consideration in the design of an aerobraked AOTV is to have an acceptable pitching stability at all possible c.g. locations at the highest allowed angle of attack. With respect to yaw and roll, the vehicle must have a neutral stability.

An aerobraked AOTV will thus fly at the highest angle of attack allowed by its pitching stability criterion (and other criteria if any; see the next section), by controlling the c.g. location. The yaw angle must be kept as close to zero as possible, so that there will be minimum interaction between yaw and roll. The roll angle will be controlled by the use of RCS engines. The effective average angle of attack and L/D can be lowered by alternating the bank angle between a positive and a negative value. A course change can be accomplished also by maintaining a fixed bank angle. In this way, the vehicle has a two-parameter control in its maneuvering.

How an aerobraked AOTV can negotiate an atmosphere with greatly varying density is yet to be determined (ref. 17). The worst situation will occur when density is distributed nonuniformly: a high density during the descent (entry) flight and low density during the ascent (exit) flight. It would be highly desirable to know the density distribution before the atmospheric flight, and that possibility is presently under study (ref. 44). A multiple atmospheric pass is suggested as one way of reducing the effect of density uncertainty (refs. 7,8,11).

Another benefit of a finite L/D is that it enables an AOTV to fly at a higher altitude than with an L/D = 0. By flying at a small negative average L/D, such as -0.1 or -0.15--by alternating the bank angle between 110° and -110° for example--the AOTV can stay within the atmosphere at higher altitudes than with an L/D = 0 (see refs. 7, 7, and 17). This will lower both the convective and radiative heat-transfer rates. Since equation (9) must be satisfied even in this case, the flight-path will become longer; but this poses no problem for an AOTV.

The multiple atmospheric pass mentioned above has one added benefit. A multiple pass results in a longer atmospheric flightpath. In order to satisfy equation (9), the vehicle must fly through an atmosphere of lower density than that in the single pass case; that is, it must fly at higher altitudes. This causes both

convective and radiative heat-transfer rates to be reduced in relation to the single-pass case (refs. 7,8).

EXAMPLES OF PROPOSED DESIGNS

Ballute

In this design, the aerobrake consists of a balloon-like elastic gas bag, inflated to the shape of a blunt body (fig. 8); it is called a ballute (combination of balloon and parachute). Its size will be varied by controlling the pressure inside the gas bag. It has been shown experimentally (ref. 45) that such a body can vary the drag coefficient over a factor of close to 2. The rocket engines could possibly be mounted on the tail side (fig. 8(a)) or at the nose side (fig. 8(b)). The main advantage of this design is that it could be the lightest and cheapest to make of all the options.

There are, however, two potential problems with the ballute. The first is that the variation of drag coefficient produces only one-degree-of-freedom control. As was mentioned in the preceding section, most of the other proposed designs have a two-degree-of-freedom control on the motion of an AOTV. A two-degree-of-freedom control would be preferable to one-degree-of-freedom control. The second possible problem concerns the question of static stability when the ballute is deformed as a result of an asymmetric external pressure distribution. No study has yet been made of the aerodynamic characteristics of a ballute that is only partially inflated and that is set at a finite angle of attack. Common sense would predict that the windward side would depress inward owing to the increased shock-layer pressure there, while the lee would bulge out because of the decreased pressure there. This will tend to produce a moment that will increase the angle of attack, leading to a static instability. To avoid the occurrence of such static instability, the location of the c.g. may have to be compromised. Therefore, a careful analysis must be carried out regarding the stability question, before serious consideration is given to the ballute scheme.

Conical Lifting Brake

In this concept, the aerobrake consists of a sphere-cone, which resembles spacecraft of past NASA missions (ref. 46). The configuration currently favored uses a 70° cone with the sphere radius equal to the frustum radius. The 70° cone was selected because it showed the largest range of allowable c.g. locations (ref. 47). This vehicle could be utilized in two ways, depending on its mission. For a delivery mission, the payload could be placed on the opposite side of the rocket engine, as shown in figure 9(a). For a retrieval mission, however, the payload would have to be on the same side as the engine (fig. 9(b)).

In addition to the fact that this design allows widest variation in the c.g. locations, it has an advantage in that the stress on the components occurs only in

one direction: the direction of rocket thrust and the direction of the aerodynamic drag coincide approximately.

The main potential problem of this design concerns the yet unknown phenomenon which somehow increases both pressure and heat-transfer rates in the base region at a finite angle of attack (ref. 48). If the phenomenon is genuine and insurmountable, this design could be used only when the distribution of density in the atmosphere is known beforehand.

Raked Cone

The raked cone is an ellipsoidal body truncated strongly asymmetrically (ref. 12), as shown in figure 10. Notice that the fuel tanks are split into two (or more) parts and are placed far apart. By controlling the relative amounts of fuel in each tank, the vehicle could adjust its trim angle of attack to a certain extent. Its optimum L/D is about 0.3, the highest of all existing designs. The high L/D makes it possible to fly at the highest negative L/D, thereby at altitudes substantially higher than 80 km. Conversely the nose radius of this vehicle can be made smaller than 10 m and still satisfy the limit on the heat-transfer rate given in table 2. The combination of the high altitude, which tends to induce the collision-limiting phenomenon mentioned earlier, and small nose radius, which tends to induce the truncation phenomenon, could cause the radiative heat-transfer rate to this body to be smaller than that given by equation (12).

There are two problems associated with the raked cone. The first is the difficulty in placing the c.g. on the thrust line of the main rocket engines; depending on the mass and dimensions of the payload and the amount of fuel remaining in the tanks, the c.g. point may vary over a wide range. Gimballing the main engines to accommodate this c.g. change will be difficult. The second problem is that the structures must withstand stresses in two directions: the direction of the thrust line when the engines are firing, and the direction of flight during atmospheric deceleration.

FLUID MECHANICS OF BASE FLOW

In both the conical lifting brake (fig. 9) and the raked cone (fig. 10), the payload may have to be carried in the base region to form a protruding afterbody, as shown in the figures. If there is any amount of heat transfer from the base flow into the protruding afterbody, then the payload may be overheated. A satellite is designed usually so that when deployed it can withstand radiative heating from the Sun and its reflection from Earth, the sum of which is about 2 kW/m^2. A deployed satellite has large protrusions such as solar cells and antennae. How these protruding parts can be folded so that they fit within the confines of the base region is yet to be determined. Whatever the solution, however, the maximum allowable heat-transfer rates to the payload are likely to be fairly small.

Convective and radiative heat-transfer rates to the base region of a reentry vehicle have been studied over the years (refs. 49-52). It is known that both convective and radiative heat-transfer rates increase with base pressure. In most past reentry vehicles, the base pressure was quite small, that is, of the order of 1% of that of the front stagnation point value (ref. 52). As a result, the base heat-transfer rates were also usually very small.

One cannot necessarily expect this to be the case for an AOTV. For the reentry vehicles studied in the past, there were no protruding afterbodies. For both the conical lifting brake and raked-cone configurations, however, there would be protruding afterbodies at the time of entry when they are used for retrieval missions. The experimental data taken in a hypersonic wind tunnel with a conical lifting brake (ref. 48) show that both pressure and convective heat-transfer rates can be very high over certain portions of the afterbody when the vehicle is at a finite angle of attack. Under certain circumstances, the convective heat-transfer rates are so high that it seems as if the flow expanding from the frustum may be hitting the afterbody to produce an oblique shock wave, or that a shock wave may be impinging on the spot (ref. 48).

In order to understand the nature of the flow in the base of a conical lifting brake, an effort is presently being made to study the phenomenon in a different type of facility. At Ames Research Center, scale models of such vehicles are flown in a hypersonic, free-flight range, and shadowgraph pictures are taken of the flow field around the flying models. The results are being analyzed with the help of computational fluid dynamics (ref. 53). A significant difference is appearing between the base flow field of this type of AOTV and that without a protruding afterbody (ref. 54). The computed flow field shows that there are two recirculating regions in the flow rather than one: one between the aerobrake and the afterbody, and the other behind the afterbody. The first recirculating region resembles a two-dimensional separated flow produced by a backward-facing step (refs. 53,54), and the second is an axisymmetric base flow. It is known that the two-dimensional separated flow over a backward-facing step produces a recirculating region pressure which is substantially higher than in the base of an axisymmetric body without protruding afterbody (refs. 52,54). Thus, one sees a possibility of relatively high base pressure for the AOTV, which may cause high convective and radiative heat-transfer rates. However, the geometrical and flow parameters under which such nearly two-dimensional behavior occurs are totally unknown.

The base flow for the raked cone has not been studied at all. One interesting aspect of this flow is the possible effect of a strong asymmetry in the base flow. In order to produce the relatively large lift coefficient inherent with this design, the flow in the base must have a substantial downward velocity component. There is a possibility even of vortices resembling wing-tip vortices, in order to accommodate this large downward velocity. The flow behavior under this configuration and its effect on the protruding payload have yet to be studied.

CONCLUSIONS

Aeroassisted orbital transfer vehicles are useful for two purposes: they can carry satellite payloads between GEOs and the Space Station, and between near-equatorial orbits and near-polar orbits on a reusable basis. Because of its reusability, high reliability resulting from the reusability, and substitution of aerodynamic forces for a rocket engine burn, the AOTVs can introduce a substantial advantage in commercial utilization of space. The flight regimes of the vehicle are defined relatively narrowly from the various practical constraints; the regimes are such that nonequilibrium vibrational excitation, dissociation, and ionization will proceed simultaneously in the shock layer over the vehicle. Present understanding of these chemical kinetic phenomena is poor. The requirement that these vehicles may have to carry their cargo in the base region, as a protruding afterbody, introduces a unique fluid-mechanical problem of base flow.

REFERENCES

1. Jane's All the World's Aircraft. Jane's Publishing Co., Vol. 1981-1982, London, England, 1982, pp. 690-691.

2. Hill, P. G.; and Peterson, C. R.: Mechanics and Thermodynamics of Propulsion. Addison-Wesley Publishing Co., Reading, Mass., 1965, p. 371.

3. Garland, S.: Integration Becomes the Name of the OTV Game. Aerospace America, vol. 22, no. 8, Aug. 1984, pp. 70-73.

4. Walberg, G. D.: A Survey of Aeroassisted Orbit Transfer. J. Spacecraft & Rockets, vol. 22, no. 1, Jan.-Feb. 1985, pp. 3-18.

5. Howe, J. T.: Introductory Aerothermodynamics of Advanced Space Transportation Systems. J. Spacecraft & Rockets, vol. 22, no. 1, Jan.-Feb. 1985, pp. 19-26.

6. Menees, G. P.: Thermal-Protection Requirements for Near-Earth Aeroassisted Orbital-Transfer Vehicle Missions. Progress in Astronautics and Aeronautics, Vol. 96, Thermal Design of Aeroassisted Orbital Transfer Vehicles, H. F. Nelson, ed., American Institute of Aeronautics and Astronautics, New York, N.Y., 1985, pp. 257-285.

7. Menees, G. P.; Park, C.; and Wilson, J. F.: Design and Performance Analysis of a Conical Aerobrake Orbital-Transfer Vehicle Concept. Progress in Astronautics and Aeronautics, Vol. 96, Thermal Design of Aeroassisted Orbital Transfer Vehicles, H. F. Nelson, ed., American Institute of Aeronautics and Astronautics, New York, N.Y., 1985, pp. 286-308.

8. Menees, G. P.; Davies, C. B.; Wilson, J. F.; and Brown, K. G.: Aerothermodynamic Heating Analysis of Aerobraking and Aeromaneuvering Orbit-Transfer Vehicles. Progress in Astronautics and Aeronautics, Vol. 96, Thermal Design of Aeroassisted Orbital Transfer Vehicles, H. F. Nelson, ed., American Institute of Aeronautics and Astronautics, New York, N.Y., pp. 338-360.

9. Menees, G. P.; Wilson, J. F.; Davies, C. B.; and Brown, K. G.: Aerothermodynamic Heating and Performance Analysis of a High-Lift Aeromaneuvering AOTV Concept. AIAA Paper 85-1060, Williamsburg, Va., 1985.

10. Powell, R. W.; Naftel, J. C.; and Stone, H. W.: Performance Evaluation of the Atmospheric Phase of an Orbital Transfer Vehicle. AIAA Paper 84-0405, Reno, Nev., 1984.

11, Rehder, J. J.: Multiple Pass Trajectories for an Aeroassisted Orbital Transfer Vehicle. Progress in Astronautics and Aeronautics, Vol. 96, Thermal Designs of Aeroassisted Orbital Transfer Vehicles, H. F. Nelson, ed., American Institute of Aeronautics and Astronautics, New York, N.Y., 1985, pp. 186-197.

12. Scott, C. D.; Reid, R. C.; Maraja, R. J.; Li, C. P.; and Derry, S. M.: An AOTV Aeroheating and Thermal Protection Study. Progress in Astronautics and Aeronautics, Vol. 96, Thermal Designs of Aeroassisted Orbital Transfer Vehicles, H. F. Nelson, ed., American Institute of Aeronautics and Astronautics, New York, N.Y., 1985, pp. 309-337.

13. Davies, C. B.; and Park, C.: Optimum Configuration of High-Lift Aeromaneuvering Orbital Transfer Vehicles in Viscous Flow. AIAA Paper 85-1059, Williamsburg, Va., 1985.

14. Beggs, J. M.: Space Station: The Next Logical Step. Aerosp. Am., vol. 22, no. 9, Sept. 1984, pp. 47-52.

15. Korb, L. J.; Morant, C. A.; Calland, R. M.; and Thatcher, C. S.: The Shuttle Orbiter Thermal Protection System. Ceramic Bulletin, vol. 60, no. 11, Nov. 1981, pp. 1188-1193.

16. Leiser, D. B.; Smith, M.; and Goldstein, H. E.: Developments in Fibrous Refractory Composite Insulation. Ceramic Bulletin, vol. 60, no. 11, Nov. 1981, pp. 1201-1204.

17. Cerimele, C. J.; and Gamble, J. D.: A Simplified Guidance Algorithm for Lifting Aeroassist Orbital Transfer Vehicles. AIAA Paper 85-0348, Reno, Nev., 1985.

18. Detra, R. W.; and Hidalgo, H.: Generalized Heat Transfer Formulae and Graphs. Research Report 72, AVCO-Everett Research Laboratories, Everett, Mass., Mar. 1960.

19. Desautel, D.: Analytical Characterization of AOTV Perigee Aerothermodynamic Regime. Progress in Astronautics and Aeronautics, Vol. 96, Thermal Design of Aeroassisted Orbital Transfer Vehicles, H. F. Nelson, ed., American Institute of Aeronautics and Astronautics, New York, N.Y., 1985, pp. 230-253.

20. Park, C.: Calculation of Radiation from Argon Shock Layers. J. Quant. Spectrosc. Radiat. Transfer, vol. 28, no. 1, July 1982, pp. 29-40.

21. Bittker, D. A.; and Scullin, J.: General Chemical Kinetics Computer Program for Static and Flow Reactions, with Application to Combustion and Shock-Tube Kinetics. NASA TN D-6586, 1972.

22. Bird, G. A.: Molecular Gas Dynamics. Clarendon Press, Oxford, England, 1976, p. 186.

23. Flagan, R. C.; and Appleton, J. P.: Excitation Mechanisms of the Nitrogen First-Positive and First-Negative Radiation at High Temperature. J. Chem. Phys., vol. 56, no. 3, Feb. 1972, pp. 1163-1173.

24. Ali, A. W.: Excitation and Ionization Cross Sections for Electron Beam and Microwave Energy Deposition in Air. Memorandum Report 4598, Naval Research Laboratory, Washington, D.C., Aug. 1981.

25. Park, C.: Calculation of Nonequilibrium Radiation in the Flight Regimes of Aeroassisted Orbital Transfer Vehicles. Progress in Astronautics and Aeronautics, Vol. 96, Thermal Design of Aeroassisted Orbital Transfer Vehicles, H. F. Nelson, ed., American Institute of Aeronautics and Astronautics, New York, N.Y., 1985, pp. 395-418.

26. Lee, J. H.: Basic Governing Equations for the Flight Regimes of Aeroassisted Orbital Transfer Vehicles. Progress in Astronautics and Aeronautics, Vol. 96, Thermal Design of Aeroassisted Orbital Transfer Vehicles, H. F. Nelson, ed., American Institute of Aeronautics and Astronautics, New York, N.Y., 1985, pp. 3-53.

27. Park, C.: Radiation Enhancement by Nonequilibrium in Earth's Atmosphere. J. Spacecraft & Rockets, vol. 22, no. 1, Jan.-Feb. 1985, pp. 27-36.

28. Park, C.: Problems of Rate Chemistry in the Flight Regimes of Aeroassisted Orbital Transfer Vehicles. Progress in Astronautics and Aeronautics, Vol. 96, Thermal Design of Aeroassisted Orbital Transfer Vehicles, H. F. Nelson, ed., American Institute of Aeronautics and Astronautics, New York, N.Y., 1985, pp. 511-537.

29. Park, C.: On convergence of Computation of Chemically Reacting Flows. AIAA Paper 85-0247, Reno, Nev., 1985.

30. Jaffe, R. L.: Rate Constants for Chemical Reactions in High-Temperature Nonequilibrium Air. AIAA Paper 85-1038, Williamsburg, Va., 1985.

31. Allen, R. A.; Rose, P. H.; and Camm, J. C.: Nonequilibrium and Equilibrium Radiation at Super-Satellite Reentry Velocities. Research Report 156, AVCO-Everett Research Laboratories, Everett, Mass., Sept. 1962.

32. Arnold, J. O.; and Whiting, E. E.: Nonequilibrium Effects on Shock-Layer Radiometry during Earth Entry. J. Quant. Spectrosc. Radiat. Transfer, vol. 13, no. 9, Sept. 1973, pp. 861-870.

33. Cauchon, D. L.: Project Fire Flight 1 Radiative Heating Experiment. NASA TM X-1222, 1966.

34. Cauchon, D. L.: Radiative Heating Results from the Fire 2 Flight Experiment at a Reentry Velocity of 11.4 Kilometers per Second. NASA TM X-1402, 1967.

35. Lee, D. B.; and Goodrich, W. D.: The Aerothermodynamic Environment of the Apollo Command Module during Super-Orbital Entry. NASA TN D-6792, 1972.

36. Whiting, E. E.; Arnold, J. O.; Page, W. A.; and Reynolds, R. M.: composition of the Earth's Atmosphere by Shock-Layer Radiometry during the PAET Entry Probe Experiment. J. Quant. Spectrosc. Radiat. Transfer, vol. 13, no. 9, Sept. 1973, pp. 837-859.

37. Evans, J. S.; Schexnayder, C. J.; and Huber, P. W.: Computation of Ionization in Re-Entry Flowfields. AIAA J., vol. 8, no. 6, June 1970, pp. 1082-1089.

38. Nerem, R. M.; and Dilley, J. F.: An Analysis of Re-Entry Flight Measurement of Shock Layer Microwave Radiation. AIAA J., vol. 8, no. 7, July 1970, pp. 1295-1301.

39. Adams, J. C., Jr.: Shock Slip Analysis of Merged Layer Stagnation Point Air Ionization. AIAA J., vol. 8, no. 5, May 1970, pp. 971-973.

40. Kang, S. W.: Nonequilibrium, Ionized, Hypersonic Flow over a Blunt Body at Low Reynolds Number. AIAA J., vol. 8, no. 7, July 1970, pp. 1263-1270.

41. Kang, S. W.; Dunn, M. G.; and Jones, W. L.: Theoretical and Measured Electron-Density Distributions for the RAM Vehicle at High Altitudes. AIAA Paper 72-689, Boston, Mass., 1972.

42. Whiting, E. E.; Arnold, J. O.; and Lyle, G. C.: A Computer Program for a Line-by-Line Calculation of Spectra from Diatomic Molecules and Atoms Assuming a Voigt Profile. NASA TN D-5088, 1969.

43. Talay, T. A.; White, N. H.; and Naftel, J. C.: Impact of Atmospheric Uncertainties and Real Gas Effects on the Performance of Aeroassisted Orbital Transfer Vehicles. Progress in Astronautics and Aeronautics, Vol. 96, Thermal Design of Aeroassisted Orbital Transfer Vehicles, H. F. Nelson, ed., American Institute of Aeronautics and Astronautics, New York, N.Y., 1985, pp. 198-229.

44. Menees, G. P.; Park, C.; Wilson, J. F.; and Brown, K. G.: Determination of Atmospheric Densityh Using a Space-Launched Projectile. AIAA Paper 85-0327, Reno, Nev., 1985.

45. Woods, W. C.; Andrews, D. G.; and Bloetscher, F.: Experimental Evaluation of an Inflatable Ballute for Application to Aeroassisted Orbital Transfer Vehicles. AIAA Paper 84-0409, Reno, Nev., 1984.

46. Intrieri, P. F.; De Rose, C. E.; and Kirk, D. B.: Flight Characteristics of Probes in the Atmosphere of Mars, Venus, and the Outer Planets. Acta Astronautica, vol. 4, no. 7-8, July-Aug. 1977, pp. 789-799.

47. Davies, C. B.; and Park, C.: Aerodynamics of Generalized Bent Biconics for Aeroassisted, Orbital-Transfer Vehicles. J. Spacecraft & Rockets, vol. 22, no. 2, Mar.-Apr. 1985, pp. 104-111.

48. Shih, P. K.; and Gay, A.: Low Lift-to-Drag Aerobrake Heat Transfer Test at Mach 10. Progress in Astronautics and Aeronautics, Vol. 96, Thermal Design of Aeroassisted Orbital Transfer Vehicles, H. F. Nelson, ed., American Institute of Aeronautics and Astronautics, New York, N.Y., 1985, pp. 378-394.

49. Murphy, S. N. B.; and Osborn, J. R.: Base Flow Phenomena with and without Injection: Experimental Results, Theories, and Bibliography. Progress in Astronautics and Aeronautics: Aerodynamics of Base Combustion, Vol. 40, S. N. B. Murphy, ed., American Institute of Aeronautics and Astronautics, New York, N.Y., 1979, pp. 345-367.

50. Park, C.: Modeling of Radiative Heating in Base Region of Jovian Entry Probe. Progress in Aeronautics and Astronautics: Entry Heating and Thermal Protection, Vol. 69, W. B. Olstad, ed., American Institute of Aeronautics and Astronautics, New York, N.Y., 1980, pp. 124-147.

51. Shirai, H.; and Park, C.: Shock-Tube Studies of Radiative Base Heating of Jovian Probe. Shock Tubes and Waves, Proceedings of the 12th International Symposium on Shock Tubes and Waves, A. Lifshitz and J. Rom, eds., Magnes Press, The Hebrew University, Jerusalem, 1980, pp. 419-428.

52. Brant, D. N.; and Nestler, D. E.: Development of an Afterbody Radiative and Convective Heating Code for Outer Planet Probes. Progress in Astronautics and Aeronautics: Outer Planet Entry Heating and Thermal Protection, Vol. 64, R. Viskanta, ed., American Institute of Aeronautics and Astronautics, New York, N.Y., 1979, pp. 345-367.

53. Lombard, C. K.; Vankatapathy, E.; and Bardina, J.: Forebody and Base Flow of a Dragbrake OTV by an Extremely Fast Single Level Implicit Algorithm. AIAA Paper 84-1699, Snowmass, Colo., 1984.

54. Chapman, D. R.; Kuehn, D. M.; and Larson, H. K.: Investigation of Separated Flows in Supersonic and Subsonic Streams with Emphasis on the Effect of Transition. NACA Technical Report R-1356, 1957.

TABLE 1.- PAYLOAD AND MASSES OF THE UPPER STAGE VEHICLE, IN kg, UNDER THE MOST IDEAL CONDITIONS, STARTING FROM AN EQUATORIAL LOW-EARTH-ORBIT AT 150 km, WITH A ROCKET ENGINE WITH A SPECIFIC IMPULSE OF 350 sec

		Space Shuttle upper stage			Ariane
Mass at takeoff from LEO assumed			30,000		4,500
Type		Expendable	OTV	AOTV	Expendable
Mass of hardware assumed		2,000	2,000	3,000	300
Delivery to GEO	Payload	7,174	2,634	4,542	1,442
	Reentry mass	0	2,000	3,000	0
Retrieval from GEO	Payload	0	1,160	8,349	0
	Reentry mass	0	3,160	11,349	0
Excursion to GEO	Payload	0	806	2,942	0
	Reentry mass	0	2,806	5,942	0

TABLE 2.- TYPICAL PERIGEE CONDITIONS FOR AEROBRAKED AOTV

Altitude, km	80
Convective heat-transfer rate q_c, kW/m^2	200
Density ρ, kg/m^3	2×10^{-5}
Mean free path λ, m	4×10^{-3}
Nose radius R, m	10
Reynolds number, $\rho VR/\mu$	1.5×10^{5}
Stagnation pressure p_s, atm	0.015
Velocity, V, km/sec	9
Viscosity μ, kg/(m·sec)	1.2×10^{-5}

	SPACE SHUTTLE (USA)	ARIANE (ESA)
LEO PAYLOAD	30,000kg	4,500kg
TAKE OFF	2,000,000kg	400,000kg

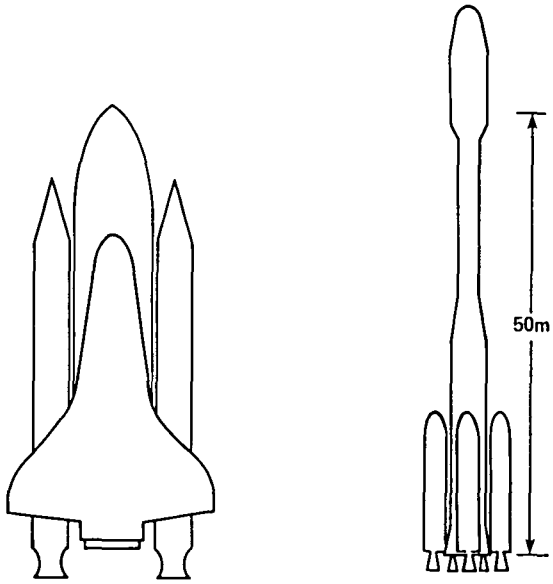

Figure 1.- Estimated approximate weights of Space Shuttle and Ariane vehicles at takeoff and of payloads at LEO at their fully developed, future stages.

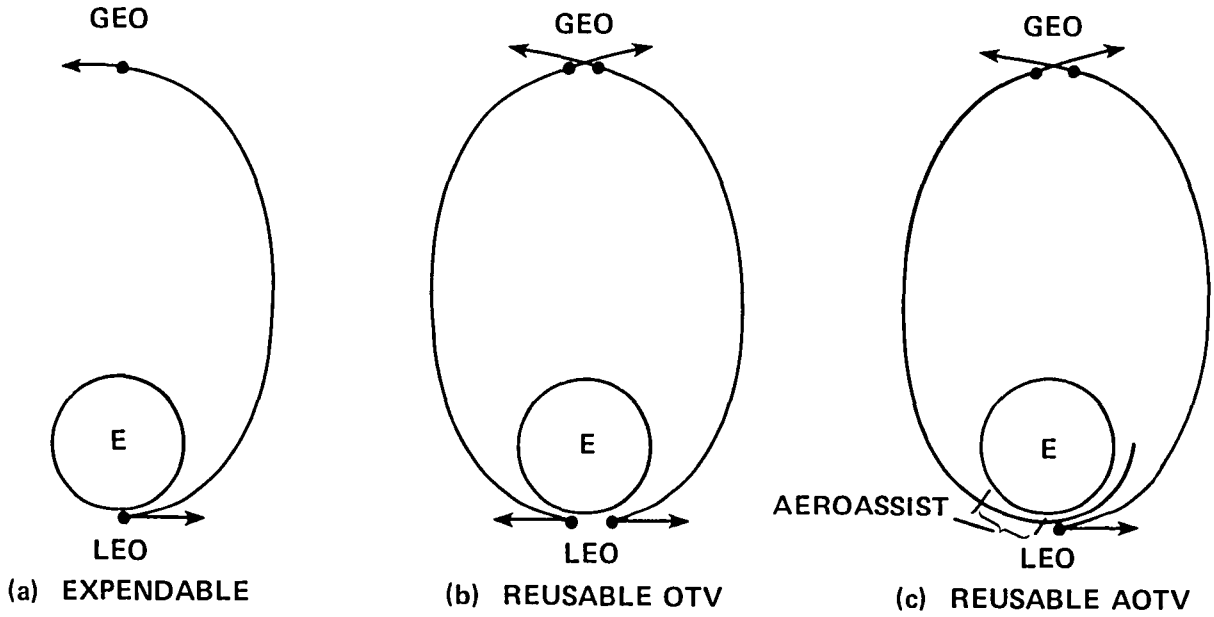

Figure 2.- Three different modes of transferring payloads from LEO to GEO.

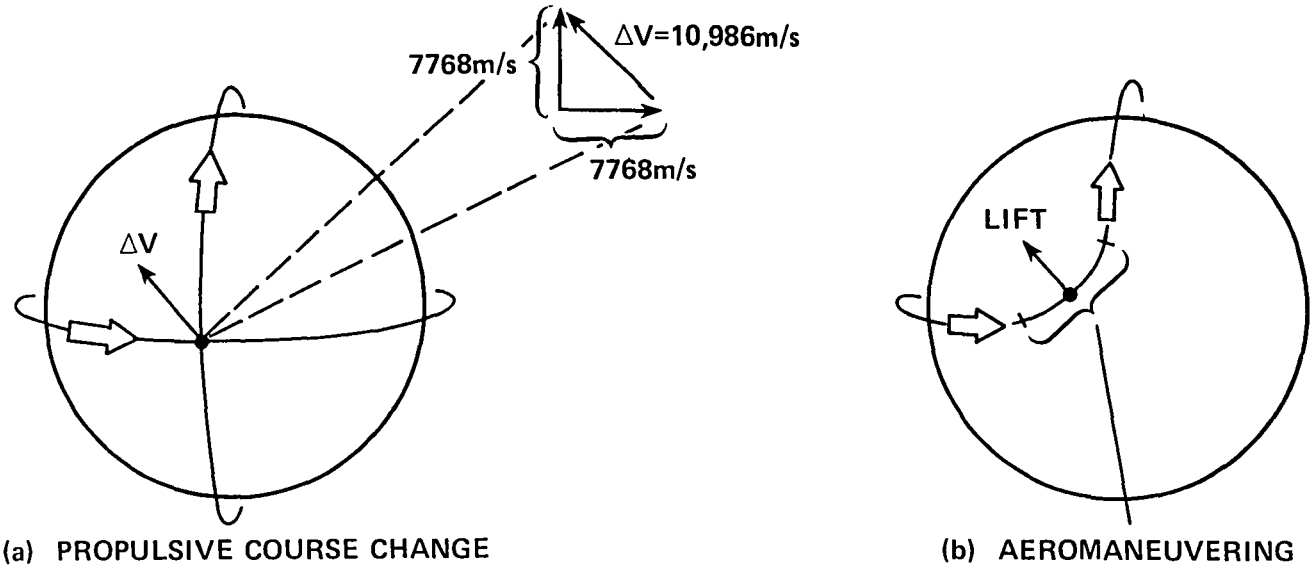

Figure 3.- Two methods of changing orbital plane inclination angle.

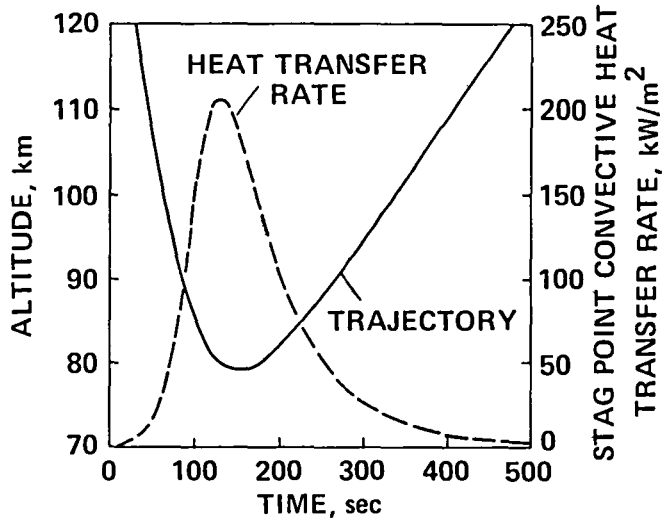

Figure 4.- Flight trajectory and stagnation point convective heat-transfer rates for a spherical aerobraking AOTV with nose radius of 10 m, mass of 10,000 kg, on return from a GEO.

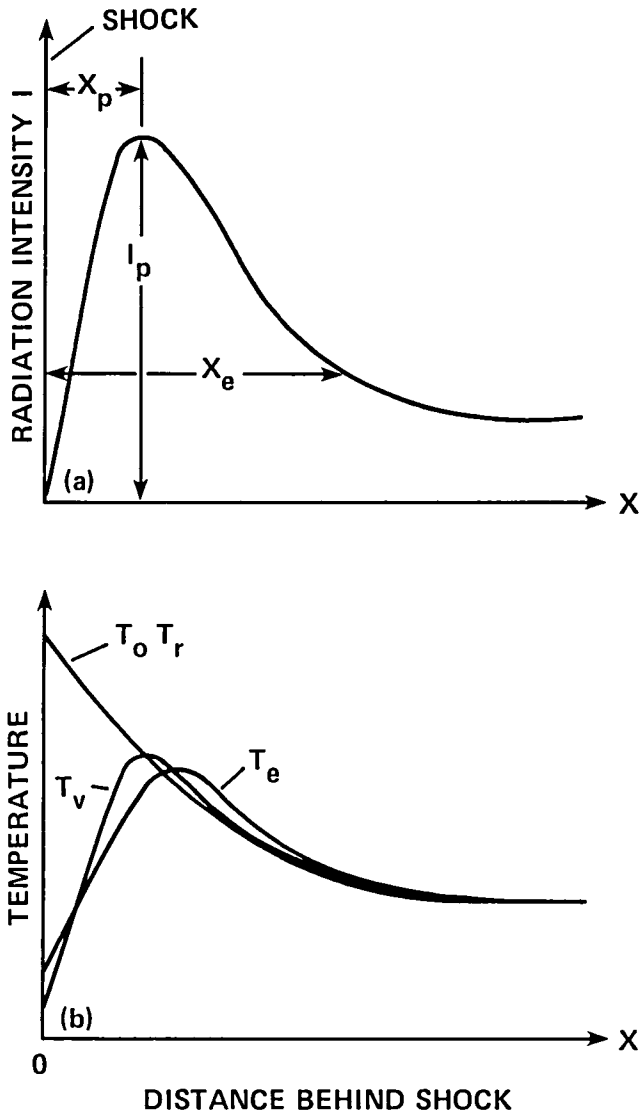

Figure 5.- Schematics of observed variation in radiation intensity from the flow behind a normal shock wave, and probable distribution of various temperatures.

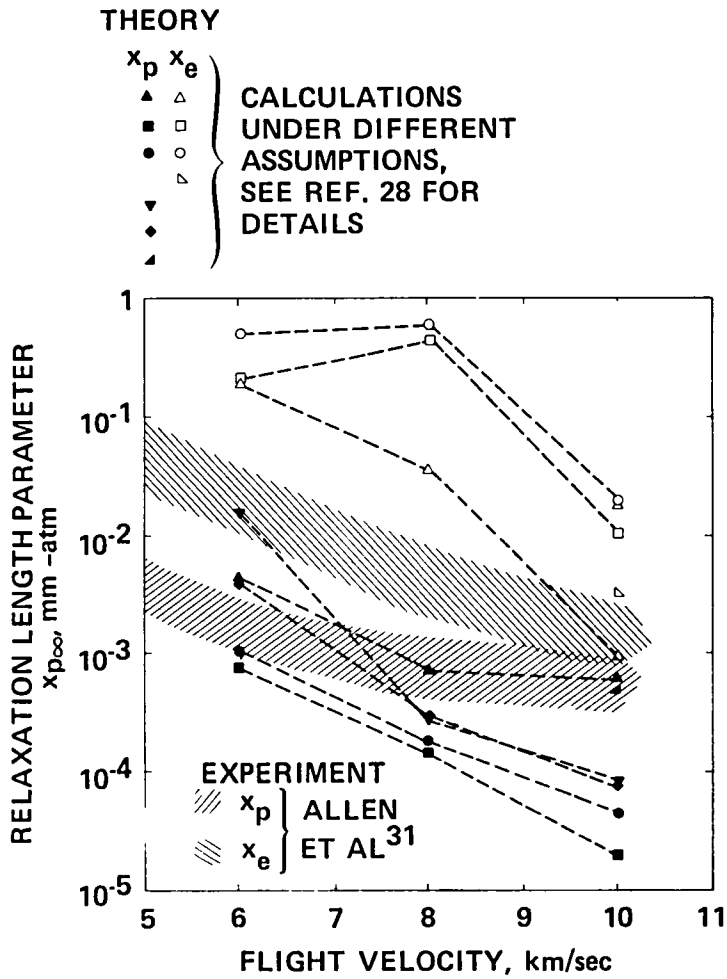

Figure 6.- Comparison of the experimental and theoretical peak radiation point x_p and equilibration point x_e (reproduced from ref. 28; see ref. 28 for detailed explanation of this figure).

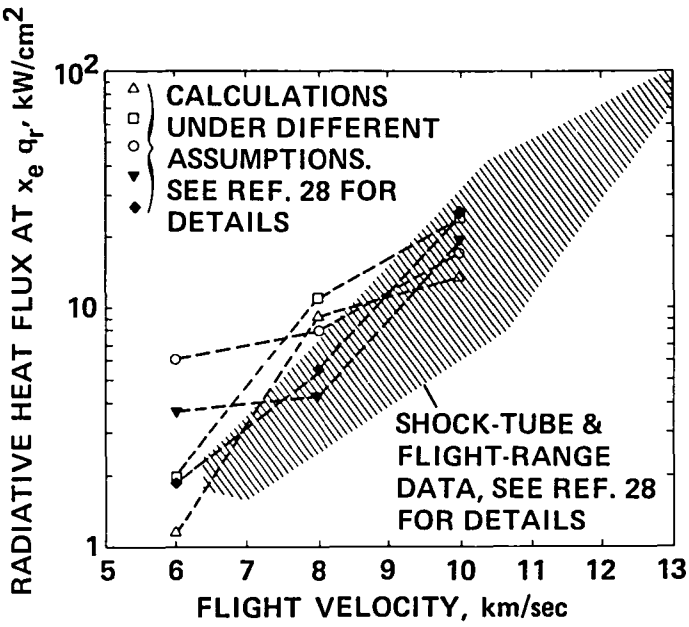

Figure 7.- Comparison of the experimental and theoretical nonequilibrium radiative heat fluxes (reproduced from ref. 28; see ref. 28 for detailed explanation of this figure).

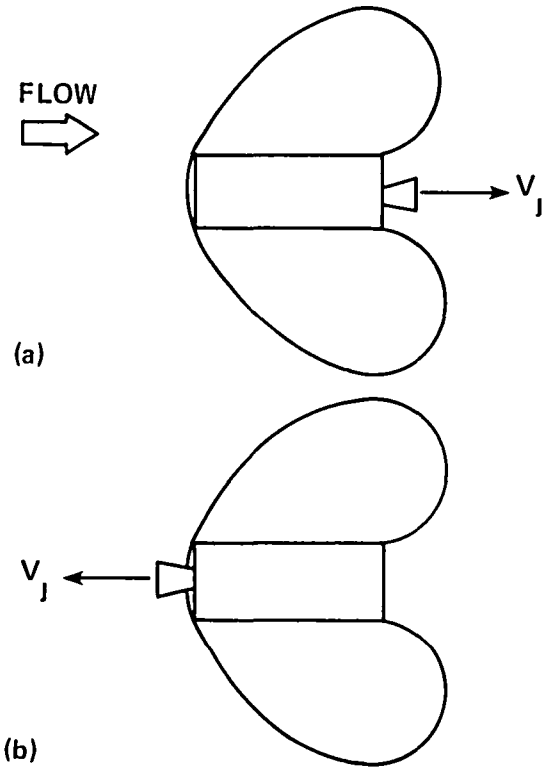

Figure 8.- Ballute configuration.

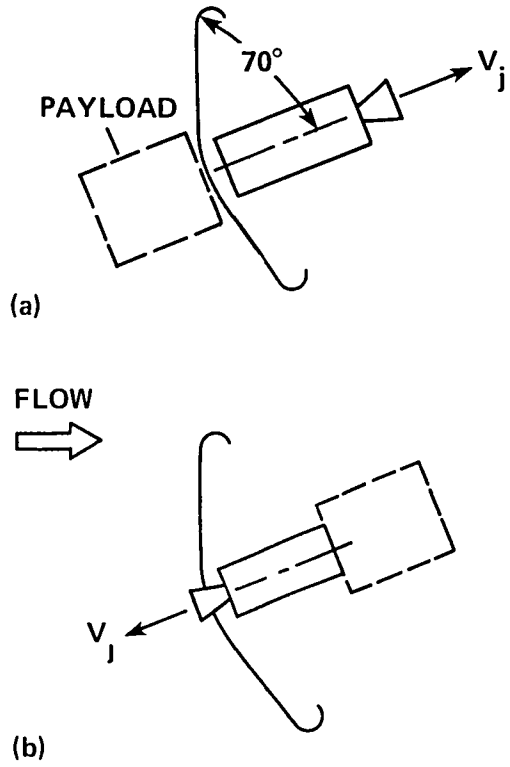

Figure 9.- Conical lifting brake configuration.

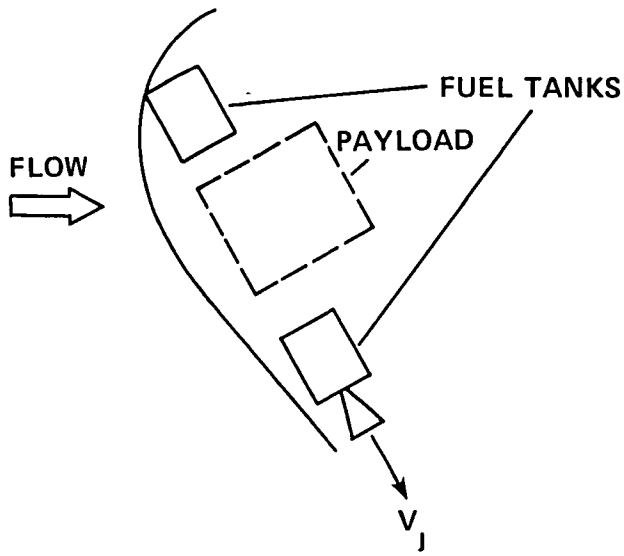

Figure 10.- Raked-cone configuration.

1 Report No	2 Government Accession No	3 Recipient's Catalog No
NASA TM-86760		

4 Title and Subtitle	5 Report Date
A REVIEW OF SHOCK WAVES AROUND AEROASSISTED ORBITAL TRANSFER VEHICLES	June 1985
	6 Performing Organization Code
7 Author(s)	8 Performing Organization Report No
Chul Park	85277
	10 Work Unit No
9 Performing Organization Name and Address	
NASA Ames Research Center Moffett Field, CA 94035	11 Contract or Grant No.
	13 Type of Report and Period Covered
12 Sponsoring Agency Name and Address	Technical Memorandum
National Aeronautics and Space Administration Washington, DC 20546	14 Sponsoring Agency Code 506-51-11

15 Supplementary Notes

Point of contact: Chul Park, Ames Research Center, MS 230-3, Moffett Field, CA 94035. (415) 694-5394 or FTS 464-5394

16 Abstract

Aeroassisted orbital transfer vehicles (AOTVs) are a proposed type of reusable spacecraft that would be used to transport cargoes from one Earth-bound orbit to another. Such vehicles could be based on the proposed Space Station and used to transport commercial satellites from the Space Station to geostationary orbits or to polar orbits and return. During a mission, AOTVs would fly through Earth's atmosphere, thus generating aerodynamic forces that could be used for decelerating the vehicles or changing their direction. This review of published AOTV research findings was concerned with the shock-wave-induced, high-temperature airflows that would be produced around these vehicles during atmospheric flight. In the survey, special emphasis was placed on the problems of (1) the chemical physics of multitemperature, ionizing, nonequilibrium air flows, and (2) the dynamics of the flows in the base region of a blunt body with complex afterbody geometry.

17 Key Words (Suggested by Author(s))	18 Distribution Statement
Aeroassisted Orbital Transfer Vehicles	Unlimited Subject Category - 16

19 Security Classif (of this report)	20 Security Classif (of this page)	21 No of Pages	22 Price*
Unclassified	Unclassified	31	A02

*For sale by the National Technical Information Service, Springfield, Virginia 22161

End of Document